

Deep Neural Networks as the Semi-classical Limit of Quantum Neural Networks

Antonino Marcianò,^{1, 2,*} Filippo Fabrocini^{*, 3, †} Enrico Greco^{*, 4, 5, ‡} and Kostas Terzidis^{3, §}

¹*Center for Field Theory and Particle Physics & Department of Physics, Fudan University, 200433 Shanghai, China*

²*Laboratori Nazionali di Frascati INFN, Frascati (Rome), Italy, EU*

³*College of Design and Innovation, Tongji University, Shanghai, China*

⁴*Institut de Chimie Radicalaire, Aix-Marseille Université, Marseille, France, EU*

⁵*College of Environmental Science and Engineering and Beijing Innovation Center for Engineering Science and Advanced Technology (BIC-ESAT), Peking University, Beijing, China*

Our work intends to show that: (1) Quantum Neural Networks (QNN) can be mapped onto spin-networks, with the consequence that the level of analysis of their operation can be carried out on the side of Topological Quantum Field Theories (TQFT); (2) Deep Neural Networks (DNN) are a subcase of QNN, in the sense that they emerge as the semiclassical limit of QNN; (3) a number of Machine Learning (ML) key-concepts can be rephrased by using the terminology of TQFT. Our framework provides as well a working hypothesis for understanding the generalization behavior of DNN, relating it to the topological features of the graphs structures involved.

I. INTRODUCTION

A paradoxical result from [1] according to which DNN memorize the training samples by brute force leaves unexplained where the generalization capabilities of DNN come from. This “apparent” paradox, as it has been dubbed by [2], has led to active discussions by many scholars such as [3], [4], [5], [6], [7], [8], [9], [10], [11], [12], [13], [14], [15]. In any case, in our vision, the overall discussion has empirically proved how far the ML community is from building a principled model of DNN and, therefore, understanding their generalization capabilities.

So far, ML techniques have been deployed in order to enhance quantum tasks ([16], [17], [18]), while Quantum Computing (QC) has been used to speed up traditional ML algorithms ([19], [20], [21], [22]). We will follow here a different perspective encompassing DNN as a sub-case (semi-classical limit) of QNN. This pathway has been suggested by the analogy with physics. A topical experiment at the base of the quantum revolution around the beginnings of the 20th century pointed out the existence of the photoelectric effect. As it is notorious, the effect has been explained by Albert Einstein resorting to a corpuscular description of the electromagnetic field, namely to the concept of photons as carriers of “quanta” of light. But, actually, the interpretation of this very seminal experiment clashed with a common perspective on quantum physics, widely spread nowadays even in the physicist’s community, and that relies on the naive assumption that quantum means microscopic and classical macroscopic. A rather different pathway consists in moving from a quantum theory, with tested semi-classical limit that corresponds to the classical theory, and investigating the varieties of predictions that can then falsify the quantum theory. This approach allows new predictive power and more robust experimental corroboration, and it is the approach we have been following within this paper.

II. MOTIVATIONS AND THEORETICAL BACKGROUND

The main inspiration for writing this paper comes from the remark that, despite the excellent performance in many different domains, the source of the success of DNN and the reason for their being powerful ML models remain elusive. DNN are still analytically opaque in the sense that they miss a principled model of their operation. This issue has a theoretical relevance and, at the same time, it is extremely urgent from an applicative point of view as well. Indeed, if we wish to trust any application making use of Deep Learning technology, we need to open the “black box” of these architectures. In this sense, a solution to a problem of this kind is also going to have a social impact to the extent it will

*Electronic address: marciano@fudan.edu.cn

†Electronic address: fabrocini@tongji.edu.cn

‡Electronic address: enrico.greco@live.it

§Electronic address: kostas@tongji.edu.cn

improve the trustworthiness of AI systems. [1] has empirically shown that successful DNN achieve 0 training error or very small error when trained on a completely random labeling of the true data. On the other side, the test error is not better than random chance insofar as there is no correlation between the training labels and the test labels. However, as the authors of the paper underline, in this case learning should have been impossible to the extent that the semantics of the training samples has been completely corrupted by the randomization of the labels, with the consequence that training should not converge or slow down substantially. Surprisingly, the training process was largely unaffected by the transformation of the labels. This result seems to leave unexplained the generalization capabilities of DNN. How to explain that DNN are actually able to achieve more than good generalization performances, even though the results of learning a function that maps an input to an output based on example input-output pairs show that the training set has been memorized by brute force?

Moreover, the output of [1] has posed a challenge to Computational Learning Theory (CoLT) as well. The experimental results emphasize that the effective capacity of several successful DNN is large enough to shatter the training data. In other words, the capacity of these models is in principle rich enough to memorize the training data (with or without the use of regularizers). In particular, the classical measures of ML model expressivity (VC-dimension, Rademacher complexity, etc.) seem to fail when explaining the capabilities of DNN. Specifically, they do not explain the good generalization behavior achieved by DNN, which are typically over-parametrized models that often have substantially less training data than model parameters [23]. As a matter of fact, it is usually understood that good generalization is obtained when a ML model does not memorize the training data, but rather learns some underlying rule associated with the data generation process, therefore being able to extrapolate that rule from the training data to new unseen data. Overfitting and, even more, brute force memorization should exclude generalization by definition, even as concerns human beings. For instance, the concepts of capacity ([24], [25], [26], [27], [28], [29], bias ([30], [31]), overfitting ([32], [33]), and generalization ([34], [35]) have been widely explored in cognitive psychology as well.

This scenario has pushed the authors of this paper to look at a different framework, the QNN framework, for revising a number of traditional ML concepts in the light of concepts coming from TQFT. At the same time the QNN framework, at least in the version we are advertising, will allow to look at DNN as the semi-classical limit of QNN and will provide a working hypothesis for understanding the generalization behavior of DNN as well as building a principled model of these computational architectures.

III. AN ILLUSTRATIVE EXAMPLE

A recurrent visual image for QNN involves nodes of the hidden layers that interconnect from each neighbor to one another. In the next sections we will instead push forward a concept of multiplicity that is based on graph theory, and that deploys the inter-connectivity of links that is proper of the topological structures. This move will allow us to rethink the generalization problem in DNN by using the QNN framework just described. As a starting point to move from, we consider a traditional feedforward architecture, as it could be used in classifying individual hand written digits (Figure 1). It is inessential to the goal of this paper to define whether an architecture of this kind will make use of backpropagation or whatever other optimization technique. In particular, we will assign a set of squared $(2j+1) \times (2j+1)$ matrices, the dimension of which is specified by half-integer numbers j , and which depend on the three Euler angles ϕ , θ and ψ , to the links and to the nodes of a graph. The assignment of $(2j+1) \times (2j+1)$ matrices to the links of the DNN is the first step required to introduce the concept of QNN we are proposing. In the next sections we will show how to reinterpret this construction in terms of specific mathematical structures that are well known in theoretical physics.

The ML task will consist in classifying individual handwritten digits. Figure 1 illustrates the three-layer neural network we could use for recognizing the individual digits. The input layer of the network will contain neurons encoding the values of the input pixels. Our training data will consist of a sample of 28×28 pixel images of scanned handwritten digits. Therefore, the input layer will contain $784 = 28 \times 28$ neurons. The input pixels are greyscale, with a value of 0.0 representing white, a value of 1.0 representing black, and the values in between representing gradually darkening shades of grey. The second layer of the network is a hidden layer. The example illustrates a hidden layer containing just $n = 15$ neurons. Finally, the output layer of the network will contain 10 neurons. We will number the output neurons from 0 through 9, and figure out which neuron has the highest activation value. If, say, the first neuron will have an output ≈ 1 , then that will indicate that the network has classified the digit as 0.

The QNN state associated to the architecture described may be recovered by: i) selecting, in the bulk of the DNN, a graph with three-valent and four-valent vertices; ii) associating to the edges interconnecting vertices $(2j+1) \times (2j+1)$ matrices labelled by either $j = 1/2$ or $j = 1$; iii) given any three-valent vertex, to the incoming or outgoing three edges of which are assigned matrices (one with dimension labelled by $j_3 = 1$ and two with dimension specified by $j_1 = j_2 = 1/2$), assigning to it a three-valent tensor saturating the indices of the matrices with the $j_1 = j_2 = 1/2$ and

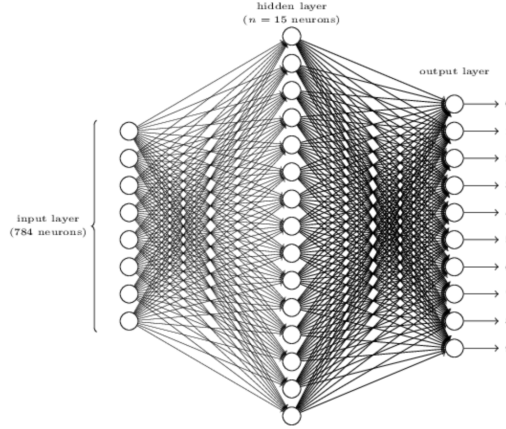


FIG. 1: A three-layers neural network for recognizing digits.

$j_3 = 1$ (Pauli matrices); iv) finally, assigning to any vertex in which four 1/2-colored edges are incoming or outgoing (three edges laying on the same layer and a fourth one external to it) a four-valent intertwiner tensor among the 1/2-colored matrices (contractions of two Pauli matrices).

IV. QUANTUM NEURAL NETWORKS

The mathematical structure on which QNN hinge is provided by Topological Quantum Field Theory (TQFT). A tight texture of analogies fetched by the equivalence among categories in quantum physics and deep machine learning specifies the theoretical perspective through which we progress. Both the Hilbert space states and the probability amplitudes describing their relative transitions are crucial to the individuation of a quantum-inspired model of QNN capable to include DNN as a specific sub-case. Following the recent literature [36], the spin-network basis of the Hilbert space states will be considered as QNN machines. These are supported on 1-complexes (graph Γ), and are endowed with a functorial evolution supported on 2-complexes. This 2-complex evolution is in turn a cobordism, which can be decomposed into a sequence of intermediate evolution operators acting between the hidden layers. As we will see, the functorial 2-complex provides the training algorithm adapted to our framework.

We consider here the illustrative case of TQFT with a local non-abelian Lie group, which we assume to be $SU(2)$ to match the example of QNN provided in the previous section. Then, squared $(2j+1) \times (2j+1)$ matrices depending on the Euler angles turn out to constitute the representations of the group elements $U \in SU(2)$. Tensors saturating, at the vertices, the matrix indices are here specified by the intertwiners of $SU(2)$. The functor, as an operator the action of which is supported on the disjoint boundary states, corresponds to the classifier (the learning rule). This is finally recovered following an association path [37], which is defined as follows:

- we integrate either twice over each internal edge in the bulk[48], or once over adjacent couple of group elements, assigned to either internal edges or vertices:

$$\begin{array}{ccc}
 \text{Diagram of a vertex with two internal edges labeled } e \text{ and one external edge labeled } U. & \Rightarrow & \int_{SU(2)} dU_{s_e} \int_{SU(2)} dU_{t_e} ;
 \end{array} \quad (1)$$

- we integrate over each couple of adjacent group element, assigned to either to a face or to an internal edge:

$$\begin{array}{ccc}
 \text{Diagram of a face with two internal edges labeled } e \text{ and one external edge labeled } f, with an intertwiner } h_{ef} \text{ between them.} & \Rightarrow & \int_{SU(2)} dU_{e*} \chi^{j_f}(U_f) ;
 \end{array} \quad (2)$$

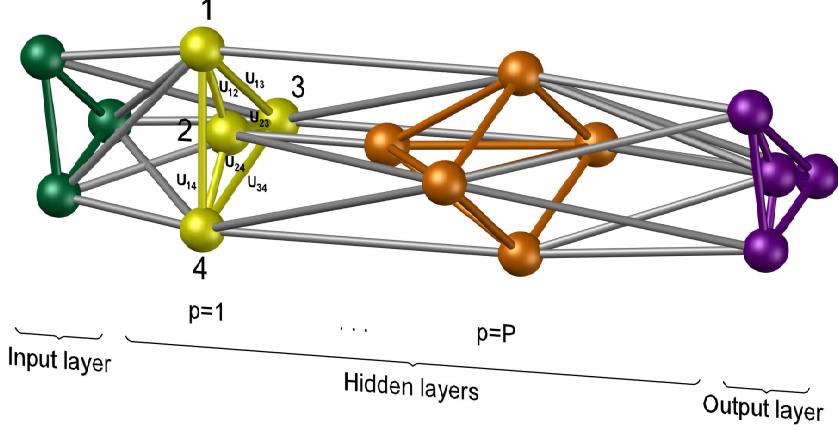


FIG. 2: A functorial evolution among two spin-network states.

- we sum over each face f^* and associate the element

$$\begin{array}{ccc} \text{Diagram of a pentagonal face } f^* & \implies & \sum_{j_{f^*}} \Delta_{j_{f^*}} \chi^{j_{f^*}} \left(\prod_{e^* \in \partial f} U_{e^*} \right); \end{array} \quad (3)$$

- we drop, at each vertex, an integral $\int_{\text{SU}(2)} dU_{v(e)}$, which appears as redundant in (1).

The functor $\mathcal{Z}(U_l)$, which provides the transition operator between boundary states and depends on the boundary group elements, acquires the expression

$$\mathcal{Z}_C(U_l) = \int_{\text{SU}(2)^{2(E-L)-V}} dU_{v(e)} \int_{\text{SU}(2)^{V-L}} dU_f \prod_f \mathcal{K}_{f^*}(U_{e^*}, U_f), \quad (4)$$

where $\mathcal{K}_{f^*}(U_{e^*}, U_f)$ denotes the “face amplitude”

$$\mathcal{K}_{f^*}(U_{e^*}, U_f) \equiv \sum_{j_{f^*}} \Delta_{j_{f^*}} \chi^{j_{f^*}} \left(\prod_{e^* \in \partial f} U_{s(e)} U_{e^*} U_{t(e)}^{-1} \right) \prod_{e^* \in \partial f} \chi^{j_{f^*}}(U_f). \quad (5)$$

Taking into account a 2-complex without boundary, (4) reduces to the partition function

$$\begin{aligned} \mathcal{Z}_C = & \int_{\text{SU}(2)^{2E-V}} dU_{v(e)} \int_{\text{SU}(2)^V} dU_f \sum_{j_{f^*}} \prod_f \Delta_{j_{f^*}} \times \\ & \chi^{j_{f^*}} \left(\prod_{e^* \in \partial f} (U_{s(e)} U_{e^*} U_{t(e)}^{-1}) \right) \prod_{e^* \in \partial f} \chi^{j_{f^*}}(U_f), \end{aligned} \quad (6)$$

where V is the sum of the valences of the faces of C . Differently than in (4), the expression in (6) provides the amplitudes of probability for the output of the transition among states.

We are finally able to specify the training algorithm of the model:

1. Initialize:

associate, between boundary states that are supported on disjoint graphs $\{\Gamma_{\text{in}}, \Gamma_{\text{out}} ; \partial C = \Gamma_{\text{out}} \cup \Gamma_{\text{in}}\}$, the functorial evolution

$$\mathcal{Z}_C(\{U_l ; l \in C\}, \{\bar{j}_l\}),$$

where $\{\bar{j}_l\}$ denote a set of parameters to be fitted in the learning process.

2. Feedforward:

2a compose a functor $\mathcal{Z}_{\mathcal{C}}(\{U_l; l \in \mathcal{C}\}, \{\bar{j}_l\})$, which is supported on a 2-complex \mathcal{C} , with a series of 2-complexes interpolating among either the intermediate hidden layers graphs or the boundary states' graphs. For P hidden layers, labelled by $p \in P$, we have the decomposition $\mathcal{C} = \mathcal{C}_1 \cup \dots \cup \mathcal{C}_p \cup \mathcal{C}_{P+1}$. Therefore

$$\begin{aligned} \mathcal{Z}_{\mathcal{C}}(\{U_l; l \in \mathcal{C}\}, \{\bar{j}_l\}) = \\ \mathcal{Z}_{\mathcal{C}_1}(\{U_{l_{\text{in}}}; l_{\text{in}} \in \Gamma_{\text{in}}\}, \{\bar{j}_{l_{\text{in}}}\}) \dots \mathcal{Z}_{\mathcal{C}_1}(\{U_{l_{\text{out}}}; l_{\text{in}} \in \Gamma_{\text{out}}\}, \{\bar{j}_{l_{\text{out}}}\}), \end{aligned}$$

where the dot denotes the integration over the group elements assigned to the interpolating graphs supporting the hidden layer structures.

2b integrate over the group elements U assigned to the hidden layer graphs, so to trace them out:

$$\begin{aligned} \mathcal{Z}_{\mathcal{C}_1}(\{G\}) \cdot \mathcal{Z}_{\mathcal{C}_2}(\{H\}) = \\ \int_{\text{SU}(2)} \prod dU \mathcal{Z}_{\mathcal{C}_1}(\{U\}, \{G\}) \mathcal{Z}_{\mathcal{C}_2}(\{U\}, \{H\}) = \mathcal{Z}_{\mathcal{C}_1 \cup \mathcal{C}_2}(\{G\}, \{H\}). \end{aligned} \quad (7)$$

This property is often referred to as a cobordism of the functorial structure.

3. Classify:

introduce $H_l \in \text{SL}(2, \mathbb{C})$, encoding the information on the set of parameters $\{\bar{j}_l\}$; by the aforementioned combinatorics, associate to the 2-complex \mathcal{C} the transition amplitude

$$\mathcal{Z}_{\mathcal{C}}(H_l) = \int_{\text{SU}(2)^{2(E-L)-V}} dU_{v(e)} \int_{\text{SU}(2)^{V-L}} dU_f \prod_f \mathcal{K}_{f*}^{t_{f*}}(U_{e*}, U_f), \quad (8)$$

where the heat kernel propagator, encoding the information about the parameter $\{\bar{j}_l\}$ through the $\text{SU}(2)$ coherent group elements [38], acquires the expression

$$\begin{aligned} \mathcal{K}_{f*}^{t_{f*}}(U_{e*}, U_f) \equiv \sum_{j_{f*}} \Delta_{j_{f*}} e^{-j_{f*}(j_{f*}+1)\frac{t_{f*}}{2}} \times \\ \chi^{j_{f*}} \left(\prod_{e* \in \partial f} (U_{s(e)} U_{e*} U_{t(e)}^{-1}) H_{e*}^{-1} \right) \prod_{e* \in \partial f} \chi^{j_{f*}}(U_f), \end{aligned} \quad (9)$$

$\{t_{f*}\}$ being a set of positive real numbers.

4. Estimate:

estimate the parameters $\{\bar{j}_l\}$, maximizing the probability derived from the amplitude $\mathcal{Z}_{\mathcal{C}}$, in a feedforward approach.

5. Repeat:

repeat the previous steps 1-4 for different choices of the boundaries $\partial\mathcal{C}$.

V. BACK TO THE ILLUSTRATIVE EXAMPLE

Before going back to the illustrative example we proposed in Sec. III, we will analyze a straightforward but illuminating simplified case, in which only 6 pixels are involved, with shades of grey that vary in the range $[0, 1]$, at decimal steps. We keep adopting irreducible representations of $\text{SU}(2)$, for uniformity with the previous cases specified. This will provide a useful insight into the proposed architecture of QNN, and favour a more structured analysis of the traditional task exposed in Sec. III.

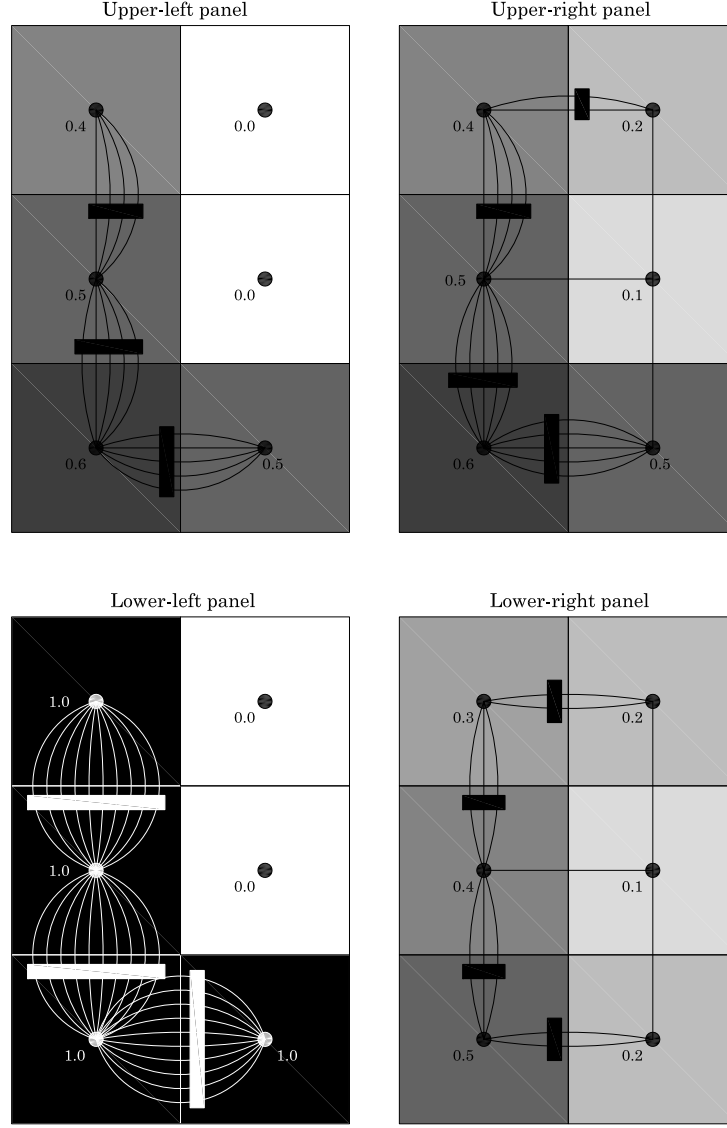


FIG. 3: Superimposed to four different images are the associated graphs, endowed with assigned $SU(2)$ irreducible representations. The bottom left panel encloses an image that corresponds exactly, i.e. with probability 1, to a "L".

A. A preliminary subcase

We shall start specifying the assignment rules for the spin j_s of the irreducible $SU(2)$ representation. These are the labels of the spin-network that capture the information of an image composed by 6 pixels. The shades of gray, ranging in $[0, 1]$, are represented by strands of irreducible representations of $SU(2)$, which are symmetrized through the Jones-Wenzl projectors [[39]], so to provide all the possible spin irreducible representations with $0 \leq j \leq 5$. We shall now imagine to associate a Delaunay triangulation to the 6 pixel image, imaging nodes positioned at the centers of each pixel, and links among the nodes. As usual, nodes are "colored" by the assignment of intertwiner quantum numbers, here intertwining among the $SU(2)$ irreducible spin j representations assigned to the links between the nodes. Between two neighboring pixels, which are characterized by two different shades of grey, in turn quantified by two different spin j irreducible representations, say j_a and j_b , we associate to the links joining the nodes at the centers of the neighboring pixels the spin representation obtained from the minimum among j_a and j_b , i.e. $j_{ab} = \min\{j_a, j_b\}$. Therefore, if one of the two neighboring pixels is white, i.e. a particular shade of grey corresponding to $j = 0$, the link among the nodes entails a spin $j = 0$ irreducible representation. In this case a spin $j = 0$ irreducible representation will be pictured in terms of the absence of any correspondent link among the nodes.

By using these simple rules, we can review a straightforward example corresponding to the recognition of the capital letter ‘‘L’’. Given an oriented frame, picturing the capital letter L requires switching on the first four pixels that are encountered while turning around, in a counterclockwise way, from the top left pixel toward the bottom ones. Now let us suppose to inspect four training examples. In the case of the first example we will assume, proceeding counterclockwise from the left top pixel, that the encountered set of shades of grey is set to be $\{0.4, 0.5, 0.6, 0.5, 0, 0\}$. The example is described by the left up panel in Figure 3. A slightly different case is represented in the right up panel of Figure 3 for which the string of numbers is $\{0.4, 0.5, 0.6, 0.5, 0.1, 0.2\}$. The ideal case, corresponding to the spin-network state that perfectly captures the letter L , with a probability $|\mathcal{A}|^2 = 1$, is given by $\{1.0, 1.0, 1.0, 1.0, 0.0, 0.0\} \equiv L$, and is represented on the left bottom panel of Figure 3. Finally, the left bottom panel represents an undetermined case captured by the string of numbers $\{0.3, 0.4, 0.3, 0.2, 0.1, 0.2\}$. We denote these cases respectively as A , B , C and D . We shall notice that these are all nothing but ‘‘colored’’ sub-graphs that can be recovered from a maximally connected graph, the one pictured in Figure 4, by removing fundamental representation strands along the links.

Spin-network basis states are represented by cylindrical functionals of the holonomies, contracted with the intertwiner invariant tensors (see e.g. A 2). A different representation involves coherent spin-network states [40], which as summarized in the previous section, can be recovered as the gauge-invariant projection of the product over links of heat kernels, namely

$$\Psi_{\Gamma, H_{ab}}(h_{ab}) = \int \left(\prod_a dg_a \right) \prod_{ab} \mathcal{K}^{t_{ab}}(h_{ab}, g_a H_{ab} g_b^{-1}), \quad (10)$$

where $a, b = 1, \dots, 6$ label the nodes of the maximal graph pictured in Figure 3, pairs ab the correspondent links, g_a $SU(2)$ group elements at the nodes, h_{ab} $SU(2)$ group elements over the links, and H_{ab} group elements of $SL(2, \mathbb{C})$, assigned to each link ab . Notice that elements of $SL(2, \mathbb{C})$ can be expressed in terms of a positive real number η_{ab} and two independent $SU(2)$ group-elements g_{ab} and g_{ab}^{-1} , namely

$$H_{ab} = g_{ab} e^{\eta_{ab}(\sigma_3/2)} g_{ba}^{-1}. \quad (11)$$

The two $SU(2)$ group elements cast uniquely in terms of an angle $\tilde{\phi}$ and a unit vector identified by its inclination and azimuth $\vec{n} = (\sin \theta \cos \phi, \sin \theta \sin \phi, \cos \theta)$. The associated $SU(2)$ group element reads

$$n = \exp(-i\phi\sigma_3/2) \exp(-i\theta\sigma_2/2), \quad (12)$$

and the $SU(2)$ group elements g recast $g = n \exp(i\tilde{\phi}\sigma_3/2)$. Thus we get

$$H_{ab} = n_{ab} e^{-iz_{ab}(\sigma_3/2)} n_{ba}^{-1}. \quad (13)$$

having introduced $z_{ab} = \xi_{ab} + i\eta_{ab}$, with $\xi_{ab} = \tilde{\phi}_{ba} - \tilde{\phi}_{ab}$. This finally allows to identify the set of six parameters, parameters associated to each link, namely $(\vec{n}_{ab}, \vec{n}_{ba}, \xi_{ab}, \eta_{ab})$. These individuate the weight vectors that are crucial to the learning process. Precisely, one six-dimensional weight vector per each link can be estimated, maximizing the transition amplitude \mathcal{A} to obtain the case D .

In particular, the state in Eq. (10) can be expanded on the spin-network basis $\Psi_{\Gamma, j_{ab}, \iota_a}$,

$$\Psi_{\Gamma, H_{ab}}(h_{ab}) = \sum_{j_{ab}} \sum_{\iota_a} f_{j_{ab}, \iota_a} \Psi_{\Gamma, j_{ab}, \iota_a}(h_{ab}), \quad (14)$$

with coefficients f_{j_{ab}, ι_a} individuated by

$$f_{j_{ab}, \iota_a} = \left(\prod_{ab} \Delta_{j_{ab}} e^{-j_{ab}(j_{ab}+1)t_{ab}} D^{j_{ab}}(H_{ab}) \right) \cdot \left(\prod_a v_{\iota_a} \right). \quad (15)$$

In the large j_{ab} limit, the coherent states $\Psi_{\Gamma, H_{ab}}(h_{ab})$ undergo the expansion

$$\Psi_{\Gamma, H_{ab}}(h_{ab}) \simeq \sum_{j_{ab}} \left(\prod_{ab} \Delta_{j_{ab}} e^{-\frac{(j_{ab}-\bar{j}_{ab})^2}{2t_{ab}}} e^{-i\xi_{ab}j_{ab}} \right) \Psi_{\Gamma, j_{ab}, \Phi_a(\vec{n}_{ab})}(h_{ab}), \quad (16)$$

where the coherent intertwiners $\Phi_a(\vec{n}_{ab})$ can be decomposed on the intertwiner space v_{ι_a} by

$$\Phi_a(\vec{n}_{ab}) = \sum_{\iota_a} \Phi_{\iota_a}(\vec{n}_{ab}) v_{\iota_a}, \quad (17)$$

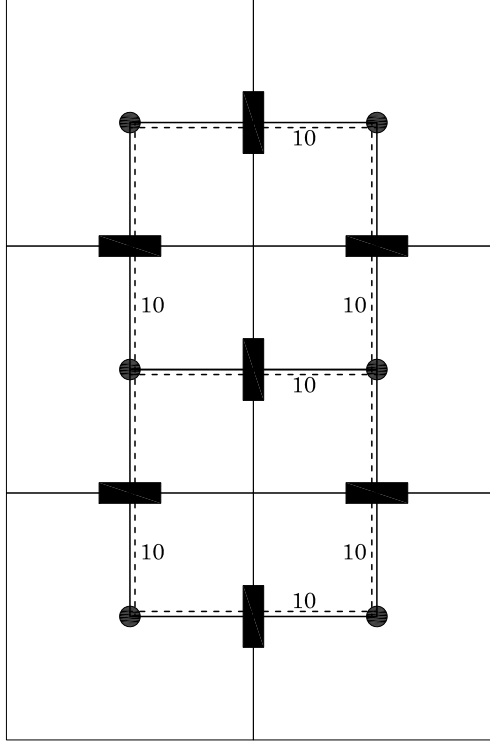


FIG. 4: The maximal graph, which encloses all the possible sub-graphs supporting the training samples' cylindrical functions.

with

$$\Phi_{\nu_a}(\vec{n}_{ab}) = v_{\nu_a} \cdot \left(\bigotimes_b |j_{ab}, \vec{n}_{ab}\rangle \right), \quad (18)$$

the variance of the Gaussian distribution per each link is inversely proportional to the diffusion time t_{ab} , namely $\sigma_{ab} \equiv 1/(2t_{ab})$, and finally the parameters \bar{j}_{ab} over which the coherent state is peaked, which correspond to the estimated parameters we refer to through the paper, are related to the η_{ab} , the real numbers entering the parametrization of $\text{SL}(2, \mathbb{C})$ group elements, at each link by $\Delta_{\bar{j}_{ab}} \equiv \eta_{ab}/t_{ab}$.

In the simplified framework of this subsection we will not take into account any hidden layer, therefore mapping our architecture on a traditional perceptron-like architecture — see e.g. [41], [42], [43]. The probability amplitude to recognize D is estimated, in the simplified framework of this subsection, simply through the internal product among the spin-network states associated to the colored graphs specified in the picture Figure 3, and the ideal graph representing the letter “L”, which is shown in the case D . In formulas, this is captured by

$$\mathcal{A}_{\prod_{ab} H_{ab}}^{(X)} = \langle \Psi_{\Gamma, H_{ab}}^{(X)} | \Psi_{\Gamma, j_{\gamma}, v_{\nu_n}}^{(D)} \rangle, \quad \text{for } X = A, B, C \quad (19)$$

which has been adapted to the fact that both the graphs are supported on the maximal graph of Figure 4. Using the

expression for the internal product of spin-networks provided in Sec. III, we finally achieve the following expression:

$$\begin{aligned}
\mathcal{A}_{\prod_{ab} H_{ab}}^{(X)} &= \langle \Psi_{\Gamma, H_{ab}}^{(X)} | \Psi_{\Gamma, j_\gamma, \iota_n}^{(D)} \rangle \simeq \sum_{jab} \left(\prod_{ab} \Delta_{jab} e^{-\frac{(j_{ab} - \bar{j}_{ab})^2}{2\sigma_{ab}^2}} e^{-i\xi_{ab} j_{ab}} \right) \\
&\quad \times \int dh_{ab} \bar{\Psi}_{\Gamma, j_{ab}, \Phi_a(\vec{n}_{ab})}(h_{ab}) \Psi_{\Gamma', j'_{ab}, v_{\iota'_a}}(h_{ab}) \\
&= \sum_{jab} \left(\prod_{ab} \Delta_{jab} e^{-\frac{(j_{ab} - \bar{j}_{ab})^2}{2\sigma_{ab}^2}} e^{-i\xi_{ab} j_{ab}} \right) \delta_{\Phi_a(\vec{n}_{ab}), v_{\iota'_a}} \delta_{j_{ab}, j'_{ab}} \\
&= \left(\prod_{ab} \Delta_{jab} e^{-\frac{(j_{ab} - \bar{j}_{ab})^2}{2\sigma_{ab}^2}} e^{-i\xi_{ab} j_{ab}} \right) \delta_{\Phi_a(\vec{n}_{ab}), v_{\iota'_a}}. \tag{20}
\end{aligned}$$

Inspecting carefully Eq. (20), we will notice that some peculiar features of QNN already appear in this simplified case. The topological structure of the graph, and the related extended information that is encoded by its links and intertwiners, are captured by the combinatorial summation of the a, b indices, and by the information stored in the Kronecker delta on the projected coherent intertwiners at each node. On the other hand, metric properties are encoded in the Gaussian weights at each link, capturing the relevant quantitative information concerning the recognition of the specific digit. It is clear that the case in which, at the link γ_{ab} , both the mean value \bar{j}_{ab} and its dispersion $(j_{ab} - \bar{j}_{ab})^2/\sigma_{ab}^2$ are vanishing, no information relatively to that link appears anymore in the amplitude, and the specific metric feature affects the topology of the graph, with the consequence that the graph will embed one link less. Finally, we recognize as a remarkable feature of this approach that probability interference terms (while computing $|\mathcal{A}|^2$) will be provided by the ξ_{ab} coefficients.

Finally, we can provide the following scheme within the perceptron framework:

1. Initialize:

1a associate to each training sample a 1-complex sub-graph of the maximal graph in Figure 4;

1b assign to each link of the 1-complex SU(2) irreducible representations.

2. Feedforward:

estimate the parameters necessary to learn the corresponding concept through the internal product of functionals associated to the sub-graphs[49];

3. Classify:

3a introduce $H_l \in \text{SL}(2, \mathbb{C})$, encoding the information on the set of parameters to be determined, namely $(\vec{n}_{ab}, \vec{n}_{ba}, \xi_{ab}, \eta_{ab})$;

3b associate to each link of the 1-complex a set of parameters, the string $(\vec{n}_{ab}, \vec{n}_{ba}, \xi_{ab}, \eta_{ab})$, to be fitted in the learning process. This identifies the functional $\Psi_{\Gamma, H_{ab}}$;

3c compute the internal product to associate probability amplitudes to the training samples:

$$\mathcal{A}_{\prod_{ab} H_{ab}} = \langle \Psi_{\Gamma, H_{ab}} | \tilde{\Psi}_{\Gamma, j_\gamma, \iota_n} \rangle, \tag{21}$$

the $\Psi_{\Gamma, H_{ab}}$ denoting the functionals of the training samples, and $\tilde{\Psi}_{\Gamma, j_\gamma, \iota_n}$ the functional associated to the image to be recognized.

4. Estimate:

estimate, for each training sample, the parameters $(\vec{n}_{ab}, \vec{n}_{ba}, \xi_{ab}, \eta_{ab})$, maximizing the probability derived from the amplitude $\mathcal{A}_{\Pi_{ab} H_{ab}}$.

These parameters individuate a rotation group element Eq. (12), which acting on a reference vector, e.g. the identity element of the SU(2) group, individuates the weight vector.

5. Repeat:

repeat the previous steps for different cylindrical functions, corresponding to different training samples, by using the estimated parameters, and the corresponding weight vectors.

estimate the new set of parameters, $(\vec{n}_{ab}, \vec{n}_{ba}, \xi_{ab}, \eta_{ab})$, thus implementing subsequent SU(2) rotations on the weight vectors.

B. Back to our illustrative example

We shall now come back to the task we introduced in Sec. III, and specify the algorithm to be adapted to it. It is worth mentioning that, with respect to the 2×3 simple digit example we analyzed in the previous section, hidden layers shall be now taken into account, consistently with the architecture specified in Sec. III. Nonetheless, this entails interpolating among intermediate states, on which a complete summation is taken into account through Eq. (7), and which are supported only on a restricted set of sub-graphs. In other words, as concerns the specific task illustrated in Sec. III, we can imagine the hidden layers to act as filtering specific patterns over others. Indeed, what the hidden layers do is to impose a selection over the intermediate graphs $\partial\mathcal{C}_n$, and hence the 2-complexes that interpolate among these latter ones. Internal summation over the irreducible representations of SU(2), namely variation of the metric properties of the QNN states, then individuates all the possible sub-graphs contained in $\partial\mathcal{C}_n$, i.e. corresponds to a variation of the topological features of the 1- and 2-complex structures.

This brings us back to the algorithm of the example in Sec. III, namely:

1. Initialize:

1a associate to each training sample a 1-complex, which is a sub-graph of the maximal graph[50] compatible with the architecture;

1b assign to each link of the 1-complex SU(2) irreducible representations[51].

2. Feedforward:

2a estimate the parameters entering the feedforward pattern through the functorial functional $\mathcal{Z}_{\mathcal{C}}(h_l)$, by maximizing the internal product \mathcal{A} between this latter and the QNN boundary states supported[52] on $\partial\mathcal{C}$;

2b compute the functorial composition (cobordism properties) to take place accordingly to Eq. (7), and consistently with the filtering process that is implemented by the selection of the sub-graph structure at each hidden layer.

3. Classify:

3a introduce $H_l \in \text{SL}(2, \mathbb{C})$, encoding the information on the set of parameters to be determined, namely $(\vec{n}_{l(s)}, \vec{n}_{l(t)}, \xi_l, \eta_l)$;

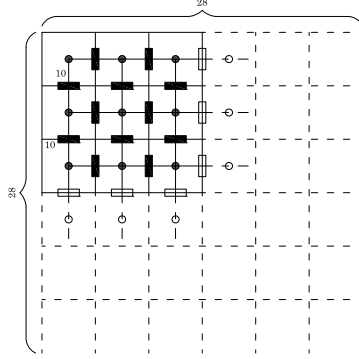


FIG. 5: The maximal graph, which encloses all the possible sub-graphs supporting the training samples' cylindrical functions for the case 28×28 pixels.

3b associate to each link l of the 1-complex, as a set of parameters to be determined, the string $(\vec{n}_{l(s)}, \vec{n}_{l(t)}, \xi_l, \eta_l)$, to be fitted in the learning process, identifying the QNN boundary state $\Psi_{\partial C, H_l}(h_l)$;

3c compute the internal product to associate probability amplitudes to the training samples, namely

$$\mathcal{A}_{\prod_l H_l} = \langle \mathcal{Z}_C | \Psi_{\partial C, H_l} \rangle, \quad (22)$$

where $\Psi_{\partial C, H_l}$ denotes the direct product of training samples and output states[53], and \mathcal{Z}_C the functorial functional interpolating among training samples and output states.

4. Estimate:

estimate, for each training sample, the parameters $(\vec{n}_{l(s)}, \vec{n}_{l(t)}, \xi_l, \eta_l)$, maximizing the probability derived from the amplitude $\mathcal{A}_{\prod_l H_l}$.

5. Repeat:

repeat the previous steps for different cylindrical functions, corresponding to different training samples: use the estimated parameters, and the corresponding weight vectors, to initialize the task; estimate the new set of parameters, $(\vec{n}_{l(s)}, \vec{n}_{l(t)}, \xi_l, \eta_l)$, thus implementing subsequent SU(2) rotations on the weight vectors.

We are now able to apply the algorithm to a restricted set of training samples, so to show how the estimate of parameters works.

VI. A DICTIONARY FOR QUANTUM NEURAL NETWORKS

As we have already mentioned, the novelty of our model consists in using the richer structures of graph-supported spin-network states to represent training and test samples. As a matter of fact, as far as we know, it is the first time that graph structures are taken into account, together with their evolution supported on 2-complexes. Instead, within the traditional approach, nodes that are located at each boundary and hidden layer, are taken to evolve along graphs (1-complexes).

Now we are ready to provide a detailed mapping of DNN notions onto QNN ones. We restrict our illustration to the supervised learning scenario consisting, as it is well known, in learning a function that maps an input X to an

output Y , based on a set of input-output pairs examples. In particular, we follow the statistical learning framework of supervised learning delineated in [44]. The notions we consider are the following, together with their respective definitions (for the sake of clarity of the readers):

- Sample complexity:
it represents the number of training-samples that a learning algorithm needs in order to learn successfully a family of target functions.
- Model capacity:
it is the ability of the model to fit a wide variety of functions; in particular, it specifies the class of functions \mathcal{H} (the hypothesis class) from which the learning algorithm can choose the specific function h .
- Overfitting:
a model is overfitting when the gap between training error and test error is too large; this phenomenon occurs when the model corresponds too closely to the training data set and may therefore fail to predict future observations reliably.
- Underfitting:
a model is underfitting when it is not able to achieve a sufficiently low error on the training set; this phenomenon occurs when the model does not adequately capture the underlying structure of the training data set and, therefore, may also fail to predict future observations reliably.
- Bias:
it is the restriction of the learning system towards choosing a classifier or predictor h from a specific class of functions \mathcal{H} (the hypothesis class).
- Empirical Risk Minimization (ERM):
it consists in minimizing the error on the set of training data (the “empirical” risk), with the hope that the training data is enough representative of the real distribution (the “true” risk).
- Generalization:
it is conceived as the ability of the learner to find a predictor which is able to enlarge successfully its own predictions from the training samples to the test or unseen samples.

These notions can be translated into the QNN dictionary as follows:

- Learner’s input:
i) the domain set X : it corresponds to links l and nodes n , and attached holonomies U_l and invariant tensors ι_n respectively along the links and at the nodes: it is concisely denoted as a state of the Hilbert space of the theory:

$$\Psi_{\Gamma; \{j_l\}, \{\iota_n\}}[A] \equiv \Psi_{\Gamma}(U_l, \iota_n) := |\Gamma; \{j_l\}, \{\iota_n\}\rangle;$$

- ii) the label set Y : it is a set of topological charges and quantum numbers, with which the 2-complex is endowed; for instance, recalling the group-isomorphism $\pi_3(S_3)$, for the mapping individuated by the homotopy group $\pi_3(S_3) = \mathbb{Z}$ the winding number w is defined as the integral over the $SU(2)$ group element

$$w = \frac{1}{24\pi^2} \int_{SU(2)} dU;$$

- iii) the training data S : it is the union of the (initial) boundary colored graphs together with the topological invariants associated to them through the QNN functorial action.

- Learner’s output:
it is a prediction rule, i.e. the QNN functor that identifies the topological charges of the boundary states (training/test samples) and thus implements the classifier; for Γ supporting a disjoint boundary state, the classifier is captured by the probability amplitude that results from the internal product

$$\mathcal{A} = \langle \Gamma; \{j_l\}, \{\iota_n\} | | \mathcal{Z}_{C, \partial C = \Gamma}; \{j_l\}, \{\iota_n\} \rangle;$$

- Sample complexity:

it is a measure of the Hilbert-space of the entire spin-network state that is supported on a specific graph Γ . It is then dependent on the connectivity of the graph (nodes and links of each graph, i.e. the multiplicity of connectivity that characterizes the graph Γ) and on the dimensionality of the Hilbert spaces connected to each link and node. In this sense complexity, once extended to the different classes of graphs corresponding to the training set, provides a measure of the entropy of the set. Therefore, in the QNN framework, the notion of “complexity” has a wider meaning than when dealing with DNN, for which the sample complexity is nothing but the size of the training set. This is summarized in the expression for the dimension of the Hilbert space \mathcal{H}_Γ of the (whole) spin-network supported on Γ , namely

$$\dim[\mathcal{H}_\Gamma] = \bigoplus_{j_l} \otimes_n \otimes_{l \in \partial n} \dim[\mathcal{H}_{j_l}];$$

- Model capacity:

it is quantified in terms of the interconnectivity of the graph Γ . It depends on the topological structure of the graphic support Γ of the spin-network states, and neither on the dimensionality of the Hilbert space of the irreducible representations nor on the intertwiner quantum numbers, respectively assigned to each link and node of Γ ; in other words, it depends on the total valence V of Γ , defined in terms of the valences v_n of each node of Γ through the expression

$$V = \sum_n v_n;$$

- Overfitting:

it depends on the topology of Γ , and it is defined in terms of the “excess” of its connectivity. The richer the connectivity, the wider the data and the information to be fitted.

- Underfitting:

it represents the converse of the overfitting scenario: the graph Γ retains reduced connectivity, less information channels (links), and lower dimensionality of the information channels (dimensions of the Hilbert space associated to each holonomy). As a consequence, the QNN cannot fit the training set and may therefore also fail to predict future observations reliably.

- Bias:

it amounts to the predisposition of the spin-network to account for a specific set of data; it depends on the topological structure of the spin-network states, encoded in the connectivity properties of Γ and on the specific realization of the QNN quantum state, i.e. on the weight of the quantum state on the spin-networks basis elements of the Hilbert space.

- Empirical Risk Minimization (ERM):

it is the variance of the Gaussian distribution of the irreducible representations assigned to the holonomies on the links, i.e.

$$\text{ERM} := \sum_l \frac{(j_l - \bar{j}_l)^2}{2L},$$

with L equal to the total number of links.

- Generalization:

it is the behavior of the system in response to test or unseen data analogous to a functor (amplitude) either from a boundary spin-network to another boundary spin-network, or from a boundary spin-network to a complex number. It is assumed to be captured by topological charges, which we divide in three classes: (i) connectivity of 1- and 2-complexes (nodes and links, vertices and edges respectively), (ii) linking and knotting (e.g. for loops in a different Hilbert space representation), and (iii) states’ sum (as a global topological charge, invariant under refinement of the triangulation, i.e. invariant under refinement of the data/group elements/intertwiners assigned to the links and the nodes). It works by selecting, in the abstract space of all the possible neural network architectures, that one which is best tailored to achieve the specific task through the topological charges that are connected. In other words, by maximizing the probability of the answer of the classifier, a specific QNN rule is learnt among all the possible QNN 2-complexes. In our specific case, the following formula summarizes this point:

$$\mathcal{Z}_C(U_l) = \int_{\text{SU}(2)^{2(E-L)-V}} dU_{v(e)} \int_{\text{SU}(2)^{V-L}} dU_f \prod_f \mathcal{K}_{f*}(U_{e*}, U_f), \quad (23)$$

where the “face amplitude” casts

$$\mathcal{K}_{f*}(U_{e*}, U_f) \equiv \sum_{j_{f*}} \Delta_{j_{f*}} \chi^{j_{f*}} \left(\prod_{e* \in \partial f} U_{e*} \right) \prod_{e* \in \partial f} \chi^{j_{f*}}(U_f). \quad (24)$$

VII. GENERALIZATION IN DNN AND TOPOLOGICAL QNN

According to the mapping between ML and QNN concepts previously illustrated, we will offer now a new perspective on the resolution of the problem as formulated by [1]. Firstly, we need to define what could look like to randomize completely the labels of the training set. In particular, we will equiparate this case to the case in which labels are generated with an approximately flat spectrum on the initial spin-network states: this will correspond to the selection of one element of the Hilbert space, with random assignment of labels.

In particular, the problem as formulated by [1] finds a natural explanation to the extent that we enlarge DNN into the richer structure of QNN (supported on graphs and endowed with topological “storage” capabilities) and understand the traditional DNN architectures as the semi-classical limit of the QNN counterparts. Since we are addressing the generalization problem in the DNN framework from the QNN side, we shall consider the coherent group elements

$$|\vec{n}, j\rangle := D^j(U_{\vec{n}}) D^j(e),$$

with e unit element of the group, \vec{n} direction on S_3 that generically individuates $U \in SU(2)$ and $D^j(e) \equiv |j, \pm \hat{z}j\rangle$.

This step allows to recover the DNN structure as the semiclassical limit of QNN. Output 1-complexes (quantum spin-networks) and 2-complexes functorial structures in order to match the classical DNN structures must be evaluated on boundary coherent group elements. Furthermore, by recognizing that (24) retains an heat kernel for the $SU(2)$ group elements, the coherent group elements can be used as a basis for the functorial structure that defines the formula

$$\mathcal{Z}_C(U_l) = \int_{SU(2)^{2(E-L)-V}} dU_{v(e)} \int_{SU(2)^{V-L}} dU_f \prod_f \mathcal{K}_{f*}(U_{e*}, U_f).$$

The same must happen for (integrated) bulk coherent group elements. The structure of QNN naturally encodes topological charges through the functorial quantum dynamics ensured by the 2-complexes, which create either vertices and then novel functions of intertwiner quantum numbers, or other topological charges encoded in the knotting and linking of the edges in the bulk of the 2-complex.

Specifically, we assume that the size of the training data is sufficient to select or, better, to learn specific paths in the boundary graph and bulk 2-complex within the most general available QNN architecture. These paths are characterized by three different types of associated non-perturbative topological charges. These latter in turn provide the sub-structures that are involved in the generalization process, as a subset supported on general 2-complexes. The topological charges that are switched on over the learning process, together with the corresponding metric properties, implement effectively the generalization process. In this sense, our approach is expected to provide a solution to the problem as raised by Zhang et al, 2016. In particular:

- the randomization of the labels of a QNN state will not induce overfitting, as a consequence of the encoding of information achieved by the QNN through the topological invariants. The quantum nature of the QNN will induce fluctuations around values of the parameters to be estimated, in a way that is compatible with the zero assumption for these parameters. This assumption would instead change the topology of the graph, and thus affect the encoding of information by the QNN. As a consequence, the disappearance of topological features of the graphs will avoid the memorization by brute force of the training samples.
- However, a DNN architecture will be trapped into an overfitting regime till memorizing the training examples by brute force, since by definition of DNN the training error vanishes — the variance for the j scale as $1/\sqrt{j}$. In other words, corresponding DNN to a set of spin-network evaluated into coherent group elements, the associated training error is zero.

Contributions to the topological invariants can be recognized to be of several different types, including the ones associated to the connectivity of the graphs, the linking and the knotting (e.g. in the loops decomposition of the QNN

boundary and intermediate spin-network states) and the states' sum invariants. The first two classes will be local in the experimental implementation of the QNN, while the latter represents a global charge, the analytical expansion of which in the deformation parameter might entail an infinite numbers of momentum expansion of the charge.

Notice that generic boundary states are characterized by two classes of parameters, which we dub as topological and metric parameters: as reminded above, the former ones are captured either by the topology of the graph, or by the topological invariant (linking and knotting) quantum numbers, which can be expressed in terms of quantum groups representations and are characterized by the deformation parameter of the quantum group, while the latter ones are captured by the spin/label of the representation itself. Whenever not enough information about the topology is specified by the training data, any QNN 2-complex with enough topological internal structure to account for the classification task will be selected. In other words, if the training data prescribe an effective shrinking of the “measure” of edges and links to zero, any topological feature of the graph, such as the valency of a node, or the knotting or linking of an edge, will cease to be. Metric parameters instead are individuated by the Gaussian weights associated to the coherent group elements assigned to the QNN states, and recovered by fit on the spin representation set that is assigned to each training state. In this sense, since the parameters fit is achieved considering the whole amplitude \mathcal{A} , the resulting topology qualifies as a derivative-free feedforward architecture in which a composition of intermediate evolution operators among the hidden layers does not need to backpropagate the information.

VIII. A NEW WORKING HYPOTHESIS

As a consequence of the previous discussions, we propose as working hypothesis for this proposal that the learning process of DNN shall be interpreted within an extended framework, which follows the very same axioms of quantum mechanics. The main idea informing the framework is that DNN should be addressed at the QNN level, and that: i) training examples or tests samples will be captured by the spin representations of the QNN quantum state, which are superpositions of the boundary Hilbert space elements; ii) the generic boundary states are characterized by two classes of parameters, which we dub topological and metric parameters: the former ones are captured either by the topology of the graph, or by the topological invariant (linking and knotting) quantum numbers, while the latter ones are captured by the spin of the representation itself; iii) about the topological parameters, information provided by the training samples, together with the definition of training error in terms of the internal product of boundary quantum states, allows to fix the functorial structure of the bulk of the QNN, namely the topological structure of the QNN 2-complex; iv) the topological parameters are enough to learn the classifier, namely the QNN 2-complex that provides the functorial structure of the QNN, playing a similar role to the frequency threshold in the photoelectric effect: whenever not enough information about the topology is specified by the training data, any QNN 2-complex with enough topological internal structure will be selected; v) metric parameters are individuated by the Gaussian weights associated to the coherent group elements assigned to the QNN states; vi) the size of the training set then will represent the analogous of the intensity of the electromagnetic field in the photoelectric effect, namely the number of photons impinging the plates of the condenser: if the size of the training set is not sufficient, i.e. it does not include enough group elements, or the training set is too noisy, links and nodes will not be sufficient to learn any classifier; vii) the “richness” or “energy” of the set of labels allows to “switch on” the links, and thus the nodes and the topological linking and knotting invariants, only for non-trivial (non-zero) values of the spin.

IX. CONCLUSIONS

Moving from the perspective of TQFT, we have shown that QNN can be mapped onto spin-networks and that DNN are a subcase of QNN, and emerge in a coherent group theoretical sense as a limit of QNN. This allowed us to establish a dictionary mapping a number of ML key-concepts on the terminology of TQFT. More importantly, we have proposed a framework that provides a working hypothesis for understanding the generalization behavior of DNN.

The novelty of our approach, particularly when compared to recent studies in the literature ([36], [45]), stands in taking into account fully, for the first time, the truly topological structure of graphs and 2-complexes on which the QNN states are supported. Indeed, ours is not only a pictorial representation, in terms of graphs, of product states belonging to the total Hilbert space (Fock space) of the theory. Instead, what we have developed is a scheme that allows to associate ML concepts to topologically invariant features of the graphs (inter-connectivity of edges, linking and knotting numbers, topological invariants on 2-complexes) and 2-complexes involved in the QNN construction.

A number of further lines of research could be pursued starting from our approach: 1. providing empirical results concerning the working hypothesis previously described; 2. defining new complexity measures more appropriate to the framework we described and adequate to explain the behavior of over-parametrized models such as DNN; 3.

introducing the notion of "time" into the architecture by modelling phenomena of the cortical plasticity such as firing rate or spike timing ([46]).

Appendix A: Topological Quantum Field Theory

We provide in this appendix a deeper introduction to Topological Quantum Field Theory (TQFT), spin-network (boundary) states and (bulk) 2-complexes functorial evolution of boundary states.

1. Classical phase-space and spin-network states

The theory is the principal $SU(2)$ -bundle over a D -dimensional base manifold \mathcal{M} . The $SU(2)$ -connection A realizes the parallel transport among infinitesimally closed fibers of the principal bundle. The parallel transport along a finite path γ connecting any two points of \mathcal{M} is individuated by

$$H_\gamma[A] = P e^{\int_\gamma A}, \quad (A1)$$

which denotes the path ordered exponential P of the integrated flux of A along γ . The holonomy then provides a group element $g \in SU(2)$. The trace of the holonomy along a closed path (a loop α) can be expanded, taking into account a squared loop of infinitesimal edge ϵ , as

$$\lim_{||\alpha|| \rightarrow 0} W_\alpha[A] = 1 - \epsilon^2 F[A] + \dots, \quad (A2)$$

where $||\alpha||$ denotes the measure of the loop α , and $F[A] = dA + A \wedge A$ is the field strength, or curvature, of the connection A . The connection A is both a 1-form on \mathcal{M} — indeed, its curvature is a 2-form over \mathcal{M} , since the differential d is one-form — and an element of the $\mathfrak{su}(2)$ algebra. Thus, it admits the decomposition over the generators τ^a , with $a = 1, 2, 3$ indices in the adjoint representation of the algebra. Consequently, the connection A and its curvature $F[A]$ acquire the dependence on the internal indices, respectively $A = A^a \tau^a$ and $F^a[A] = dA^a + \epsilon^{abc} A^b \wedge A^c$, the Levi-Civita symbol ϵ^{abc} providing the structure constants of $SU(2)$ and the Einstein convention of summing repeated indices is intended.

A TQFT can be introduced considering the topological action associated to the Lagrangian density function

$$\mathcal{L}[A] = B^a \wedge F^a[A] = \text{Tr}[B \wedge F[A]], \quad (A3)$$

where the B field denotes a $\mathfrak{su}(2)$ algebra valued D -form, which is the canonically conjugated momentum to the connection A , and the trace over the generators of the algebra is normalized to the identity and yields $\text{Tr}[\tau^a \tau^b] = \delta^{ab}$. The phase-space variables A and B can be then paired in a symplectic construction, imposing the Poisson brackets

$$\{A_a^i(x_1), B_j^b(x_2)\} = \delta_a^b \delta_i^j \delta(x_1, x_2), \quad (A4)$$

with $i = 1, \dots, D$ space indices over the dimensions of \mathcal{M} .

Holonomies realize the smearing of the configuration space variables, i.e. the connections A , along the paths γ . Similarly, the smearing of the frame fields B can be implemented by substituting their fluxes calculated through the surfaces Σ of co-dimension 1 that crosses the paths γ at least in one point, namely

$$B_\Sigma = \int_\Sigma B \cdot n, \quad (A5)$$

where n is the normal to the surface Σ and the dot denotes contraction of indices. For example, since the dimension of the path γ is 1, its co-dimension 1 surface in a 3D ambient space will be a 2D surface.

The theory we just introduced retains what is called a gauge symmetry, namely a symmetry under internal transformations, which individuates an equivalence class that describes an observer. These are instantiated by transformations involving generic group elements $g \in SU(2)$, i.e.

$$A \rightarrow A_g = g^{-1} A g + g^{-1} d g, \quad (A6)$$

and

$$B \rightarrow B_g = g^{-1} B g. \quad (A7)$$

It is trivial to check that the action (A3) is invariant under the joined action of (A6)-(A7). The infinitesimal expansion of finite transformation rules (A6)-(A7) can be cast at the $\mathfrak{su}(2)$ algebraic level, through the infinitesimal expansion of a group element around the identity, i.e. $g \simeq \mathbb{1} + \alpha^a \tau^a + \dots$. This individuates an infinitesimal transformation

$$\delta_\alpha B = [B, \alpha], \quad \delta_\alpha A = \mathcal{D}_A \alpha, \quad (\text{A8})$$

where the commutators $[,]$ denote the adjoint action of the algebra. The generators of the algebra appear in $B = B^a \tau^a$ and $\alpha = \alpha^a \tau^a$, while \mathcal{D}_A denotes the covariant $\text{SU}(2)$ derivative $\mathcal{D}_A := d + A$.

Another symmetry, which is relevant for the definition of TQFT, is the shift symmetry. This is actually ensuring the theory under consideration to be topological, as it is straightforward to recognize by looking at

$$B \rightarrow B + \delta_\eta B, \quad \delta_\eta B = \mathcal{D}_A \eta, \quad (\text{A9})$$

and

$$A \rightarrow A + \delta_\eta A, \quad \delta_\eta A = 0, \quad (\text{A10})$$

where η is any arbitrary infinitesimal 0-form (a function). Under the infinitesimal transformations (A13)-(A15), the variation of the action of the theory $\mathcal{S}[A] = \int_{\mathcal{M}} \mathcal{L}[A]$, namely

$$\delta_\eta \mathcal{S}[A, B] = \mathcal{S}[A + \delta_\eta A, B + \delta_\eta B] - \mathcal{S}[A, B], \quad (\text{A11})$$

vanishes, due to the Bianchi identity $\mathcal{D}_A F[A] = 0$. This latter identity appears in the variation of the action due to an integration by part:

$$\begin{aligned} \int_{\mathcal{M}} \text{Tr}[(B + \delta_\eta B) \wedge F[A + \delta_\eta A]] &= \int_{\mathcal{M}} \text{Tr}[(B + \mathcal{D}_A \eta) \wedge F[A]] = \\ \int_{\mathcal{M}} \text{Tr}[B \wedge F[A]] - \int_{\mathcal{M}} \text{Tr}[B \wedge \eta \mathcal{D}_A F[A]] &= \int_{\mathcal{M}} \text{Tr}[B \wedge F[A]]. \end{aligned} \quad (\text{A12})$$

This symmetry is often referred to as a “gauge symmetry” of the BF theory, which individuates a class of equivalence among physical solutions that differ by this transformation.

On the other hand, the equation of motions are specified by the variation of the action with respect to the phase-space fields:

$$\mathcal{D}_A B = 0, \quad F[A] = 0. \quad (\text{A13})$$

Solutions are then “flat”, or with zero curvature, i.e. $F[A] = 0$, while the frame fields satisfy the Gauß constraint $\mathcal{D}_A B = 0$, which generates the gauge transformations. Locally, by the topological shift symmetry, any frame field B that satisfies the Gauß constraint can be recast as $\mathcal{D}_A \eta$, for some η . This is true as locally closed forms are exact, and continue to satisfy the Gauß constraint. This implies that locally the solutions of the equations of motion belong to the same equivalence class, modulo gauge transformations and shift symmetry transformations. Since these can be mapped into vanishing configurations, this argument finally shows that there are no propagating degrees of freedom in BF theories, namely that these theories are topological.

2. Graph-kinematics

As a last step before proceeding to the definition of the 1- and 2-complexes, we introduce the irreducible representations of the group, the so-called “spin” numbers, and the inter-twiner numbers, depending on the $\text{SU}(2)$ recoupling theory. At this purpose, we remind that in this case holonomies over a path γ are group elements of $\text{SU}(2)$, and thus undergo the transformations

$$H_\gamma[A] \rightarrow g_{s(\gamma)}^{-1} H_\gamma[A] g_{t(\gamma)}, \quad (\text{A14})$$

where $g_{s(\gamma)}$ and $g_{t(\gamma)}$ are group elements assigned respectively to the source and the target of an oriented path γ . For $\text{SU}(2)$, irreducible representation of holonomies are provided by the Wigner matrices and labelled by the semi-integer j -spin numbers, namely

$$D^{(j_\gamma)}(U_\gamma), \quad U_\gamma \equiv H_\gamma[A], \quad (\text{A15})$$

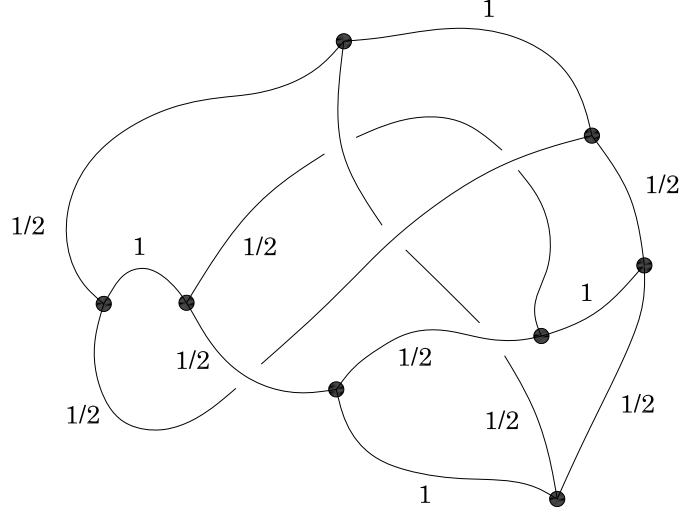


FIG. 6: A graph with tri-valent nodes colored under $SU(2)$.

$SU(2)$ intertwiners are expressed as the (group elements) integrals of a number of copies of irreducible representations (Wigner matrices). As a compact group, $SU(2)$ is endowed with a Haar measure (invariant under gauge transformations and coordinate reparametrizations) that enables the definitions of the intertwiner invariant tensors. These latter quantities can be thought to be associated to the nodes where endpoints (target points) and origins (source points) of the paths γ intersect. A collection of n path $\gamma_1, \gamma_2 \dots \gamma_n$ intersecting at their target and source points (nodes) provides a graph Γ . The internal indices of the Wigner matrices integrated ensure gauge-invariance through the contraction with the holonomies flowing across the node. Integrating in the Haar measure the irreducible representations of the holonomies, the target or source points of which cross at the node, and which are labelled by the spin $j_{\gamma_1}, j_{\gamma_2} \dots j_{\gamma_n}$, provided the expression for the inter-twiner

$$v_\iota = \int_{SU(2)} dU D^{(j_{\gamma_1})}(U) D^{(j_{\gamma_2})}(U) \dots D^{(j_{\gamma_n})}(U), \quad (A16)$$

having again suppressed all the (intertwiner and Wigner matrices) representation indices.

A collection of holonomies, the internal indices of which are contracted with the intertwiners defined by integration of the group elements at the nodes, defines a spin-network state. In terms of its constituents, the holonomies and the intertwiners, a spin-network state cast as

$$\psi_{\Gamma, \{j_\iota\}, \{\iota_n\}}[A] = \left(\bigotimes_{n \in \Gamma} v_{\iota_n} \right) \cdot \left(\bigotimes_{\gamma \in \Gamma} D^{j_{\gamma_l}}(U_{\gamma_l}[A]) \right), \quad (A17)$$

where the dot denotes the contraction of internal indices, and $l = 1, \dots, n$ label the n paths γ that compose the graph Γ .

$SU(2)$ spin-network states are equipped with a Haar measure, which ensures invariance under gauge transformations and diffeomorphisms (coordinate reparametrizations) on the base manifold \mathcal{M} , of the internal product

$$\langle \Psi_{\Gamma', j_{\gamma}, \iota_n'}[A] | \Psi_{\Gamma, j_{\gamma}, \iota_n}[A] \rangle = \delta_{\{\Gamma'\}, \{\Gamma\}} \delta_{j_{\gamma}, j_{\gamma}} \delta_{\iota_n', \iota_n} \quad (A18)$$

Invariance under diffeomorphisms, which is expressed by the Kronecker delta between classes of equivalence of graphs endowed with the same topology, namely $\{\Gamma\}$, instantiates the symmetry under elastic transformations, rendering the graph structure truly topological. In this study, graphs Γ are also referred to as 1-complexes.

3. Graph-dynamics

A concept of dynamics requires the definition of boundary states (1-complexes), the quantum evolution of which is provided by relative transition amplitudes. These are captured by the path integral (realizing the vacuum-vacuum

transition, with no underlying graph structure) and the expectation values in its measure. It is convenient to introduce the mathematical concept of 2-complex \mathcal{C} . A 2-complex \mathcal{C} is composed by edges e departing or ending either at nodes $n \in \Gamma$ or at vertices v internal to \mathcal{C} , by faces f bounded by either links γ or internal edges e , and vertices v where edges cross. We are going to show how to associate a functor — either the partition function $Z_{\mathcal{C}}[U_{\gamma}]$, or the expectation value of boundary state in the path-integral associated to the topological theory — to a 2-complex \mathcal{C} endowed with boundary group elements U_{γ} .

The partition function for the BF model over a $SU(2)$ -bundle is specified by the expression

$$\mathcal{Z} = \int \mathcal{D}AB e^{\imath \int_{\mathcal{M}} \text{Tr}[B \wedge F]} = \int \mathcal{D}A \delta(F). \quad (\text{A19})$$

where in the last equality we introduced a Dirac delta measure on the space of flat connections. This is understood [47] from smearing the phase-space variables and then casting the partition function as

$$\mathcal{Z}(\Delta) = \int_{\mathfrak{su}(2)^E} \prod_{e \in E} dB_e \int_{\text{SU}(2)^{E^*}} \prod_{e \in E^*} dU_e e^{\imath \sum_{e \in \Delta} \text{Tr}[B_e F_e]}, \quad (\text{A20})$$

where Δ denotes the triangulation of the manifold \mathcal{M} — this allows to introduce a simplicial complex Δ^* that is dual to the triangulation Δ — E denotes the set of edges e of the triangulation Δ , and E^* the set of edges e^* of the dual simplicial complex Δ^* . Furthermore, in the expression (A20) we have been using the natural definition of the curvature, which is expressed by the product of group elements U_{e^*} associated to the links around the boundary ∂f^* of a dual face f^* (thus associated with the dual face itself):

$$U_{f^*} = \prod_{e^* \in \partial f^*} U_{e^*}. \quad (\text{A21})$$

where $F_e = \ln U_{e^*}$, namely individuates a Lie algebra element that entails the discretization of the connection field curvature on the edges e of Δ . Integration over the algebra elements B_e provides the expression for the Dirac delta on the product of group elements that realizes the smearing of the curvature, namely

$$\int_{\mathfrak{su}(2)^E} \prod_{e \in E} B_e e^{\imath \sum_{e \in \Delta} \text{Tr}[B_e F_e]} = \delta(e^{F_e}) = \delta(U_{f^*}). \quad (\text{A22})$$

The partition function then casts

$$\mathcal{Z}(\Delta) = \int_{\text{SU}(2)^{E^*}} \prod_{e \in E^*} dU_{e^*} \prod_{f^*} \delta(U_{f^*}). \quad (\text{A23})$$

This formula finally admits a re-manipulation in terms of the irreducible representation of $SU(2)$, which thanks to the Peter-Weyl expansion, is provided by Plancherel formula

$$\delta(U_{f^*}) = \sum_{j_{f^*}} \Delta_{j_{f^*}} \chi^{j_{f^*}}(U_{f^*}), \quad (\text{A24})$$

where j_{f^*} denote half-integer numbers that label $SU(2)$ irreducible representations, $\Delta_j = (2j + 1)$ the dimension of these latter, and $\chi^j(U) = D^j(U)_{\alpha}^{\alpha}$ is the character of the group element $U \in SU(2)$, i.e. the trace of a Wigner matrix over the internal indices α in the representation Hilbert space. Then the partition function recasts

$$\mathcal{Z}(\Delta) = \sum_{j_{f^*}} \int_{\text{SU}(2)^{E^*}} \prod_{e \in E^*} dU_e \prod_{f^*} \text{Tr}[D(\prod_{e^* \in \partial f^*} U_{e^*})], \quad (\text{A25})$$

which depends only on the recoupling theory of $SU(2)$, and retains a dependence on the dimension of the manifold \mathcal{M} , in which both the graphs Γ and the 2-complex \mathcal{C} are merged. Thus, we can identify the no-boundary path-integral amplitude $\mathcal{Z}(\Delta)$ with the no-boundary functor $\mathcal{Z}_{\mathcal{C}}$, i.e.

$$\mathcal{Z}_{\mathcal{C}} = \mathcal{Z}(\Delta) \quad (\text{A26})$$

where there is no dependence on the boundary group elements.

[1] C. Zhang, S. Bengio, M. Hardt, B. Recht, and O. Vinyals (2016), cs/1611.03530.

[2] K. Kawaguchi, L. P. Kaelbling, and Y. Bengio (2017), 1710.05468.

[3] N. S. Keskar, D. Mudigere, J. Nocedal, M. Smelyanskiy, and P. T. P. Tang, *On large-batch training for deep learning: Generalization gap and sharp minima* (2016), 1609.04836.

[4] D. Arpit, S. Jastrzkebski, N. Ballas, D. Krueger, E. Bengio, M. S. Kanwal, T. Maharaj, A. Fischer, A. C. Courville, Y. Bengio, et al., in *Proceedings of the 34th International Conference on Machine Learning, ICML 2017, Sydney, NSW, Australia, 6-11 August 2017*, edited by D. Precup and Y. W. Teh (PMLR, 2017), vol. 70 of *Proceedings of Machine Learning Research*, pp. 233–242, arXiv:1706.05394, URL <http://proceedings.mlr.press/v70/arpit17a.html>.

[5] L. Dinh, R. Pascanu, S. Bengio, and Y. Bengio (2017), 1703.04933.

[6] G. K. Dziugaite and D. M. Roy (2017), 1703.11008.

[7] E. Hoffer, I. Hubara, and D. Soudry (2017), 1705.08741.

[8] D. Krueger, N. Ballas, S. Jastrzebski, D. Arpit, M. S. Kanwal, T. Maharaj, E. Bengio, A. Fischer, and A. Courville (2017), Workshop track-ICLR 2017.

[9] B. Neyshabur, S. Bhojanapalli, D. McAllester, and N. Srebro, in *Advances in Neural Information Processing Systems* (2017), pp. 5947–5956.

[10] B. Neyshabur, S. Bhojanapalli, and N. Srebro (2017), 1707.09564.

[11] L. Wu, Z. Zhu, and W. E, *Towards understanding generalization of deep learning: Perspective of loss landscapes* (2017), 1706.10239.

[12] R. Shwartz-Ziv and N. Tishby (2017), 1703.00810.

[13] H. W. Lin, M. Tegmark, and D. Rolnick, *Journal of Statistical Physics* **168**, 1223–1247 (2017), ISSN 1572-9613.

[14] A. Wang, H. Zhou, W. Xu, and X. Chen (2017), 1708.05029.

[15] J. Li, Y. Sun, J. Su, T. Suzuki, and F. Huang (2020), 2001.05070.

[16] N. B. Lovett, C. Crosnier, M. Perarnau-Llobet, and B. C. Sanders, *Physical review letters* **110**, 220501 (2013).

[17] M. Tiersch, E. Ganahl, and H. J. Briegel, *Scientific reports* **5**, 12874 (2015).

[18] G. Carleo and M. Troyer, *Science* **355**, 602 (2017), ISSN 0036-8075.

[19] E. Aïmeur, G. Brassard, and S. Gambs, *Machine Learning* **90**, 261 (2013).

[20] G. D. Paparo, V. Dunjko, A. Makmal, M. A. Martin-Delgado, and H. J. Briegel, *Physical Review X* **4**, 031002 (2014).

[21] M. Schuld, I. Sinayskiy, and F. Petruccione, *Quantum Information Processing* **13**, 2567 (2014).

[22] A. Kapoor, N. Wiebe, and K. Svore, in *Advances in Neural Information Processing Systems 29*, edited by D. D. Lee, M. Sugiyama, U. V. Luxburg, I. Guyon, and R. Garnett (Curran Associates, Inc., 2016), pp. 3999–4007, URL <http://papers.nips.cc/paper/6401-quantum-perceptron-models.pdf>.

[23] I. Goodfellow, Y. Bengio, and A. Courville, *Deep Learning*, Adaptive Computation and Machine Learning series (MIT Press, 2016), ISBN 9780262035613, URL <https://mitpress.mit.edu/books/deep-learning>.

[24] G. A. Miller, *Psychological review* **63**, 81 (1956).

[25] W. D. Wattenmaker, G. I. Dewey, T. D. Murphy, and D. L. Medin, *Cognitive Psychology* **18**, 158 (1986).

[26] R. L. Lewis, *Journal of psycholinguistic research* **25**, 93 (1996).

[27] N. Cowan, *Behavioral and brain sciences* **24**, 87 (2001).

[28] J. Feldman, *Nature* **407**, 630 (2000).

[29] J. Zhu, B. R. Gibson, and T. T. Rogers, in *Advances in neural information processing systems* (2009), pp. 2322–2330.

[30] T. L. Griffiths, B. R. Christian, and M. L. Kalish, *Cognitive Science* **32**, 68 (2008).

[31] T. L. Griffiths, Generalization of knowledge: Multidisciplinary perspectives pp. 135–156 (2010).

[32] R. C. O’reilly and J. L. McClelland, *Hippocampus* **4**, 661 (1994).

[33] W. K. Vong, A. Hendrickson, A. Perfors, and D. J. Navarro, in *CogSci* (2016).

[34] R. N. Shepard, *Science* **237**, 1317 (1987).

[35] A. Jern and C. Kemp, in *Proceedings of the Annual Meeting of the Cognitive Science Society* (2009), vol. 31.

[36] E. Farhi and H. Neven (2018), 1802.06002.

[37] C. Rovelli, *J. Phys. Conf. Ser.* **314**, 012006 (2011), 1010.1939.

[38] E. Bianchi, E. Magliaro, and C. Perini, *Phys. Rev. D* **82**, 124031 (2010), 1004.4550.

[39] L. Kauffman, S. Lins, and S. Lins, *Temperley-Lieb Recoupling Theory and Invariants of 3-manifolds*, Annals of Mathematics Studies (Princeton University Press, 1994), ISBN 9780691036403, URL <https://books.google.co.vi/books?id=ZSE1jwEACAAJ>.

[40] E. Bianchi, E. Magliaro, and C. Perini, *Phys. Rev. D* **82**, 024012 (2010), 0912.4054.

[41] M. Schuld, I. Sinayskiy, and F. Petruccione, *Physics Letters A* **379**, 660 (2015).

[42] A. J. da Silva, T. B. Ludermir, and W. R. de Oliveira, *Neural Networks* **76**, 55 (2016).

[43] K. H. Wan, O. Dahlsten, H. Kristjánsson, R. Gardner, and M. Kim, *npj Quantum information* **3**, 1 (2017).

[44] S. Shalev-Shwartz and S. Ben-David, *Understanding machine learning: From theory to algorithms* (Cambridge university press, 2014).

[45] K. Beer, D. Bondarenko, T. Farrelly, T. J. Osborne, R. Salzmann, D. Scheiermann, and R. Wolf, *Nature communications* **11**, 1 (2020).

[46] P. J. Sjöström, G. G. Turrigiano, and S. B. Nelson, *Neuron* **32**, 1149 (2001).

[47] J. C. Baez, *Lecture Notes in Physics* p. 25–93 (2000).

[48] For bulk we intend any 2-complex structure, without boundary. Therefore $Z_C[U_{\gamma_l}]$ acts in a functorial way on the boundary states, which are 1-complexes, i.e. colored graphs Γ composed by a collection of paths γ and nodes where the paths intersect, to which are assigned respectively holonomies and intertwiners.

[49] The functorial composition among hidden layers is no longer present in this task, since we are dealing with a perceptron

framework.

- [50] This generalizes the procedure employed to find the maximal graph for the examples dealt with in the previous subsection, i.e. the graph in Figure 4, by association of nodes to the centers of the training samples' pixels, for 28×28 pixels images
- [51] In this case, involving shades of grey that vary, at decimal steps, in the range $[0, 1]$, the assignment is identical to the case treated in the previous subsection. Such an assignment identifies the metric properties of the graph.
- [52] Support for QNN boundary states are graphs resulting from the disjoint union of any Γ' , on which training samples are constructed, and 1-complexes supporting output states.
- [53] This can be trivially an image to be recognized, as in the previous subsection.